High-throughput platform for depolarization-induced Ca^{2+} release for skeletal muscle disease mutation validation and drug discovery

Takashi Murayama[1*], Nagomi Kurebayashi[1], Takuro Numaga-Tomita[2], Takuya Kobayashi[1], Satoru Okazaki[1], Kyosuke Yamashiro[1], Tsutomu Nakada[2], Shuichi Mori[3], Ryosuke Ishida[3], Hiroyuki Kagechika[3], Mitsuhiko Yamada[2], Takashi Sakurai[1]

[1]Department of Pharmacology, Juntendo University School of Medicine, Tokyo, Japan.

[2]Department of Molecular Pharmacology, Shinshu University School of Medicine, Matsumoto, Japan.

[3]Institute of Biomaterials and Bioengineering, Tokyo Medical and Dental University, Tokyo, Japan.

[*]Corresponding author: Takashi Murayama, Ph.D., Department of Pharmacology, Juntendo University School of Medicine, Tokyo 113-8421, Japan. E-mail: takashim@juntendo.ac.jp

Abstract

In skeletal muscle excitation-contraction (E-C) coupling, depolarization of the plasma membrane triggers Ca^{2+} release from the sarcoplasmic reticulum (SR), referred to as depolarization-induced Ca^{2+} release (DICR). DICR occurs via the type 1 ryanodine receptor (RyR1), which physically interacts with the dihydropyridine receptor Cav1.1 subunit in specific machinery formed with additional components. Exome sequencing has accelerated the discovery of many novel mutations in DICR machinery genes in various skeletal muscle diseases. However, functional validation is time-consuming because it must be performed in a skeletal muscle environment. Here, we describe a high-throughput platform for DICR that is reconstituted in non-muscle HEK293 cells. We demonstrate that Cav1.1 mutations implicated in malignant hyperthermia and myopathy exhibit divergent effects on DICR. We also tested several RyR1 inhibitors and DICR modulators. This high-throughput DICR platform will accelerate validation of mutations and drug discovery for skeletal muscle diseases.

32 **Introduction**

33 In vertebrate skeletal muscle, depolarization of the plasma membrane triggers Ca^{2+} release from
34 the sarcoplasmic reticulum (SR), which is commonly referred to as excitation-contraction (E-
35 C) coupling. This process occurs at triad junctions in which a transverse (T) tubule is closely
36 apposed to terminal cisterna of the SR[1]. In excitation-contraction coupling, the type 1 ryanodine
37 receptor (RyR1), a Ca^{2+} release channel in the SR, is activated by a conformational change of
38 the voltage sensor in the Cav1.1 subunit of the dihydropyridine receptor (DHPR) upon
39 depolarization of the T-tubule membrane. This is referred to as depolarization-induced Ca^{2+}
40 release (DICR)[2,3]. Studies with knockout animals have revealed that functional and structural
41 interactions between Cav1.1 and RyR1 in muscle require at least three additional components,
42 a β1a auxiliary subunit of DHPR[4,5], the Stac3 adaptor protein[6,7,8], and junctophilins[9], which
43 may form specific machinery for DICR[4,5,10].

44 Mutations in genes that encode DICR machinery components have been implicated in
45 various types of muscle diseases, including congenital myopathies, periodic paralysis, and
46 malignant hyperthermia (MH)[11,12,13]. Rapid exome sequencing has accelerated the discovery of
47 novel mutations; however, validation of these mutations by functional testing is critically
48 important for the diagnosis and treatment of these diseases. This has been performed using
49 myotubes from mice that lack DICR machinery components, for example knockout mice of
50 Cav1.1[14], β1a[15] and Stac3[16]. While this approach has evaluated several disease-causing
51 mutations in the DICR components [16–20], it has certain limitations. For example, it is expensive
52 and labor intensive to maintain the mouse lines. Differentiation of cells into myotubes is time
53 consuming and is affected by various factors, such as the cell line used and experimental
54 conditions. Furthermore, transduction of foreign genes into myotubes is often inefficient.

55 There are no specific treatments for most diseases related to mutations in the DICR
56 machinery. A major cause for the slow pace of novel drug development is the lack of an
57 appropriate drug screening platform for these diseases. We have recently established an efficient
58 high-throughput platform for screening RyR1-targeted drugs using endoplasmic reticulum (ER)
59 Ca^{2+} measurements in HEK293 cells[21,22] and using this platform we developed Compound 1
60 (Cpd1), a novel RyR1 inhibitor for treatment of MH[23,24]. Therefore, functional screening using
61 HEK293 cells is a promising platform for drug discovery.

62 Recently, Perni et al.[25] successfully reconstituted DICR by co-expressing five essential
63 components, RyR1, Cav1.1, β1a, junctophilin-2 (JP2) and Stac3, in non-muscle tsA201 cells.

They demonstrated formation of ER-plasma membrane junctions in which Cav1.1 is arranged into tetrads, which is indicative of physical links to RyR1[26]. Depolarization of the plasma membrane using the patch-clamp technique induced a rapid Ca^{2+} transient without influx of extracellular Ca^{2+}. This provides a basis for developing reconstituted DICR.

In this study, we established a high-throughput platform for DICR that was reconstituted in HEK293 cells. Baculovirus infection of essential components greatly improved transduction efficiency. Chemical depolarization by expression of an inward-rectified potassium channel (Kir2.1) and high concentration potassium [K^+] solutions enabled the simultaneous stimulation of many cells. Furthermore, a genetically-encoded ER Ca^{2+} indicator quantitatively measured DICR without influence of extracellular Ca^{2+} influx. Using this platform, we successfully evaluated disease-causing mutations in Cav1.1 and tested several RyR1 inhibitors and DICR modulators. Our high-throughput platform will accelerate the validation of mutations and drug discovery for skeletal muscle diseases.

Results

Establishment of a high-throughput platform for DICR using a fluorescence microplate reader

To reconstitute DICR, we used HEK293 cells stably expressing RyR1 and R-CEPIA1er, a genetically-encoded fluorescent ER Ca^{2+} indicator[27], that were generated for high-throughput screening of novel RyR1 inhibitors[21,22] (**Fig. 1a**, left). The other components for DICR, Cav1.1, β1a, Stac3 and JP2, which were used by Perni et al.[25], were transduced using VSV-G pseudotyped baculovirus (BV), which efficiently infects mammalian cells[28,29] (**Fig. 1a**, right). In these cells, DICR can be detected by a decrease in ER Ca^{2+}. To prevent extracellular Ca^{2+} influx through Cav1.1 by depolarization, a N617D mutation was introduced that abolishes Ca^{2+} conductance[30]. In addition, we expressed Kir2.1, an inward-rectified potassium channel in skeletal muscle[31], to hyperpolarize the membrane potential because the resting membrane potential in HEK293 cells is much less (−20 mV) than in skeletal muscle (−90 mV)[32]. Imunocytochemistry revealed that the five proteins (Cav1.1, β1a, Stac3, JP2, and Kir2.1) were successfully expressed in almost all cells, which we term hereafter 5 BV cells (**Supplementary Fig. 1a**). BV-dependent protein expression was also confirmed by western blotting of cell lysate (**Supplementary Fig. 1b**). Therefore, BV infection effectively transduced the essential components of DICR in RyR1/R-CEPIA1er-HEK293 cells.

95 To detect DICR, we used a fluorescence microplate reader (FlexStation3), which
96 measures time-lapse R-CEPIA1er fluorescence in 96-well plates. Fluorescence signals were
97 collected in a 1.5 mm diameter area; therefore, an averaged signal from thousands of cells was
98 detected in each well. We adopted chemical depolarization using high [K^+] solutions, which
99 can simultaneously depolarize all the cells to trigger DICR. The cells were initially incubated
100 with normal Krebs solution containing 5 mM K^+. Then, solutions containing various K^+
101 concentrations were added to give K^+ concentrations of 5–61 mM. In cells without BV infection,
102 no apparent changes in fluorescence were observed with any change in [K^+] (**Fig. 1b**). Caffeine
103 (10 mM) reduced the R-CEPIA1er fluorescence, confirming the functional expression of RyR1.
104 In 5 BV cells, high [K^+] solution rapidly reduced the R-CEPIA1er fluorescence in a [K^+]-
105 dependent manner (**Fig. 1c**). To monitor ER Ca^{2+} changes in individual cells, we also observed
106 R-CEPIA1er fluorescence using laser scanning confocal microscopy. In 5 BV cells, high [K^+]
107 solution caused a large and transient reduction in the R-CEPIA1er fluorescence in 90% of cells
108 (**Movie S1** and **Supplementary Fig. 2**).

109 For quantitative analysis, we normalized the averaged fluorescence intensity of the last
110 25 seconds (F) to that of the initial 25 seconds (F_0) to correct variations in the initial
111 fluorescence intensity between wells. The F/F_0 plot as a function of K^+ concentrations
112 demonstrated K^+ dependence with an EC_{50} of ~10 mM K^+ (**Fig. 1d**). The initial fluorescence
113 change after stimulation (i.e., 35 seconds) may reflect the rate of Ca^{2+} release. However,
114 variations were too large to accurately determine the EC_{50} values because of rapid changes in
115 fluorescence intensity (**Supplementary Fig. 3**). The fluorescence change by 61 mM K^+, which
116 is expressed as $1-F/F_0$ (**Fig. 1d**), reached ~80% of that induced by caffeine in 5 BV cells,
117 indicating a high degree of DICR reconstitution (**Fig. 1e**). Taken together, these results indicate
118 successful establishment of a high-throughput platform for DICR.

119 The original method for DICR reconstitution monitors cytoplasmic [Ca^{2+}][25]; therefore,
120 we also assessed DICR by measuring cytoplasmic Ca^{2+} using G-GECO1.1, a genetically-
121 encoded Ca^{2+} indicator[33]. In cells without BV infection, a substantial increase in [Ca^{2+}] was
122 observed by high [K^+], indicating the existence of endogenous Ca^{2+} influx pathways by
123 depolarization (**Supplementary Fig. 4a**). In 5 BV cells, DICR was detected by rapid and large
124 increases in [Ca^{2+}] (**Supplementary Fig. 4b**). However, [Ca^{2+}] rapidly declined with time. This
125 may be caused by Ca^{2+} extrusion pathways in HEK293 cells. The transient nature of the [Ca^{2+}]
126 rise and substantial background make it difficult to quantitatively measure DICR by
127 cytoplasmic [Ca^{2+}] in our platform.

128 **Validation of the reconstituted DICR**

129 We next determined whether the reconstituted platform reproduces DICR in skeletal
130 muscle. Initially, we examined the role of the essential components. Removal of Cav1.1 resulted
131 in complete loss of high [K^+]-induced Ca^{2+} release (**Fig. 2a, b**). Ca^{2+} release was also lost in
132 cells lacking β1a or Stac3, and in cells expressing RyR2 instead of RyR1 (**Fig. 2b**). Removal
133 of JP2 significantly reduced the fluorescence change by 61 mM K^+ with a large rightward shift
134 in K^+ dependence (**Fig. 2a, b**). These results are consistent with previous findings of mice
135 lacking each component[9,14–16,34].

136 Skeletal muscle Cav1.1 forms a complex with three auxiliary subunits, β1a, α_2-δ and γ_1[35].
137 β1a is essential for DICR, while α_2-δ and γ_1 may play modulatory roles[36]. Additional expression
138 of α_2-δ had no effect on high [K^+]-induced Ca^{2+} release (**Fig. 2c, d**). Expression of γ1 did not
139 significantly affect high [K^+]-induced Ca^{2+} release at 20 mM or lower [K^+] but it reduced the
140 fluorescence change at higher K^+ concentrations (**Fig. 2c, d**). In γ_1 cells, R-CEPIA1er
141 fluorescence decreased but increased again with time, suggesting inactivation of the Ca^{2+}
142 release (**Supplementary Fig. 5**). These findings are consistent with previous reports of the
143 effects of α_2-δ[37] and γ_1[38] on DICR. Therefore, our reconstituted platform can reproduce DICR
144 in skeletal muscle and is valid for evaluating disease-causing mutations or drugs.

145 We also tested the importance of Kir2.1. Removal of Kir2.1 completely abolished high
146 [K^+]-induced Ca^{2+} release with substantial reduction in the R-CEPIA1er fluorescence intensity
147 (**Fig. 3a–c**). We quantified resting ER [Ca^{2+}] by determining the maximum fluorescence
148 intensity of R-CEPIA1er using ionomycin/Ca^{2+} (**Supplementary Fig. 6**). The resting ER [Ca^{2+}]
149 was severely reduced in cells without Kir2.1 (**Fig. 3d**). The resting membrane potential of 5
150 BV cells was polarized in normal Krebs solution and became depolarized by high [K^+] solution
151 containing 50 mM K^+ in the presence of ~145 mM intracellular K^+ (**Fig. 3e**). In contrast, resting
152 membrane potential was already depolarized in the cells without Kir2.1 in normal Krebs
153 solution. We hypothesized that spontaneous DICR activity under the depolarized conditions
154 causes ER Ca^{2+} depletion. In support of this idea, further removal of β1a or Stac3, which
155 completely abolishes DICR activity, restored the ER [Ca^{2+}] (**Fig. 3d**). Therefore, Kir2.1 is
156 indispensable for our reconstituted DICR platform.

157 **Evaluation of disease-causing mutations in Cav1.1**

158 Using the high-throughput DICR platform, we evaluated mutations in Cav1.1 which

159 are implicated in various muscle diseases[12,39]. We initially tested known MH mutations,
160 R174W[40], R1086H[41], and T1354S[19] (**Fig. 4a**). We found that ER [Ca^{2+}] was severely reduced
161 for R1086H (**Fig. 4b**) and that R1086H exhibited a smaller fluorescence change in response to
162 high [K^+] (**Fig. 4c, d**) compared with the wild type (WT) or the other mutants. This was partly
163 caused by low ER [Ca^{2+}], which reduces maximum fluorescence changes. In addition, R1086H
164 showed an enhanced K^+-dependence, i.e., lower EC_{50} value for K^+ (**Fig. 4c, e**). In contrast, no
165 or only minor changes in ER Ca^{2+} and K^+ dependence were observed for R174W and T1354S
166 cells (**Fig. 4b–e**). We anticipated that the reduction in ER [Ca^{2+}] in R1086H cells was caused
167 by spontaneous activation of Cav1.1 at resting membrane potential because of its
168 hypersensitivity. To test the hypothesis, we hyperpolarized the membrane potential which
169 reduced the spontaneous activation of Cav1.1. Reduction of [K^+] in the Krebs solution from 5
170 mM to 2.5 mM successfully hyperpolarized the membrane potential by ~15 mV
171 (**Supplementary Fig. 7a**). This substantially increased ER [Ca^{2+}] in R1086H cells to a level
172 comparable to that in WT cells (**Supplementary Fig. 7b**). R1086H cells exhibited a clear
173 greater sensitivity to K^+ than WT cells (**Supplementary Fig. 7c–e**), supporting our hypothesis
174 of R1086H hyperactivation.

175 Previous functional characterization of these Cav1.1 mutants consistently showed
176 enhanced caffeine sensitivity, i.e., acceleration of Ca^{2+}-induced Ca^{2+} release (CICR)[17–19]. We
177 tested caffeine dependence of these mutants in our platform. Caffeine released Ca^{2+} from WT
178 cells in a dose-dependent manner (**Fig. 4f**). R1086H cells also exhibited a caffeine dependence
179 but with reduced fluorescence change by 61 mM K^+ (**Fig. 4g**) and a significantly smaller EC_{50}
180 (**Fig. 4h**), indicating an enhanced caffeine sensitivity. In contrast, caffeine dependence was not
181 changed in R174W or T1354S cells (**Fig. 4f–h**).

182 We next examined the effect of myopathy-related mutations in Cav1.1 on DICR
183 activity. We chose four mutations, E100K, F275L, P742Q, and L1367V[42], none of which have
184 been functionally characterized (**Fig. 5a**). ER [Ca^{2+}] was not changed by any of these mutations
185 (**Fig. 5b**). DICR activity was completely lost in the F275L mutant (**Fig. 5c, d**) and there was a
186 substantial rightward shift in K^+ dependence for P742Q (**Fig. 5c**); The EC_{50} value was threefold
187 higher in P742Q (33.2 ± 1.0 mM) compared with WT (10.3 ± 0.9 mM) (**Fig. 5e**). The other two
188 mutations (E100K and L1367V) had no significant effects on K^+ dependence (**Fig. 5c-e**). We
189 also tested the effects of these mutations on caffeine-induced Ca^{2+} release. No substantial
190 changes were observed with any of the mutations (**Fig. 5f–h**).

191 **Effect of drugs on DICR activity**

192 The high-throughput DICR platform is expected to be useful for screening drugs for
193 muscle diseases. To test this possibility, we examined the effects of known DICR modulators.
194 We initially tested three RyR1 inhibitors (**Fig. 6a**). Dantrolene is a well-known RyR1 inhibitor
195 that is clinically used for MH[43]. Cpd1 is a novel potent RyR1-selective inhibitor that we recently
196 developed[23,24]. Procaine inhibits CICR but not DICR in frog skeletal muscle[44,45]. Dantrolene
197 (10 μM) and Cpd1 (3 μM) caused rightward shifts in K^+ dependence compared with the control,
198 indicating that they inhibit DICR (**Fig. 6b, c**). This is consistent with the suppression of twitch
199 and tetanic tension in isolated muscles and of reduced *in vivo* muscle weakness by
200 dantrolene[46,47] and Cpd1[24]. Procaine (5 mM), in contrast, did not inhibit DICR (**Fig. 6b, c**). All
201 three compounds shifted the caffeine dependence rightward, indicating inhibition of CICR (**Fig.**
202 **6d, e**). These results indicate that dantrolene and Cpd1 inhibit both DICR and CICR, whereas
203 procaine is a CICR-selective inhibitor.

204 Lyotropic anions, such as perchlorate and thiocyanate, potentiate E-C coupling in
205 skeletal muscle[48–52]. Perchlorate (10 mM) and thiocyanate (10 mM) significantly shifted the K^+
206 dependence leftward (**Fig. 7a, b**). In contrast, they did not affect caffeine dependence (**Fig. 7c,**
207 **d**). These results indicate that lyotropic anions potentiate DICR but not CICR. This is consistent
208 with previous findings showing that the potentiating effects of lyotropic anions are primarily
209 caused by shifting voltage dependence of the charge movement toward more negative
210 potentials[48–52]. Taken together, our high-throughput platform reproduces the effects of known
211 DICR modulators, indicating that it can be used to screen for and test drugs that affect DICR.

212 **Discussion**

213 In this study, we established a high-through platform for DICR that was reconstituted in
214 HEK293 cells expressing RyR1 and R-CEPIA1er. We made three key improvements to the
215 original method by Perni et al. [25]. First, the essential components were transduced using VSV-
216 G pseudotyped baculovirus, which can effectively infect a wide variety of mammalian cells
217 without toxicity[28]. This greatly increased the transduction efficiency; almost all cells expressed
218 the essential components (**Supplementary Fig. 1**). Second, depolarization of the plasma
219 membrane was induced by high [K^+] solution. This enabled us to simultaneously stimulate
220 many cells (**Fig. 1, Supplementary Fig. 2** and **movie S1**). For this purpose, we expressed
221 Kir2.1, an inward-rectifying potassium channel, which effectively hyperpolarized the
222 membrane potential [32] (**Fig. 3**). Third, ER [Ca^{2+}], instead of cytoplasmic [Ca^{2+}], was measured

223 to detect DICR. This is critically important to avoid contamination of signals from extracellular
224 Ca^{2+} influx. Indeed, ER [Ca^{2+}] was not changed by high [K^+] depolarization in cells without
225 essential components (**Fig. 1a**). In contrast substantial increases in cytoplasmic [Ca^{2+}] were
226 observed (**Supplementary Fig. 4a**). These improvements allow quantitative measurements of
227 DICR using a microplate reader.

228 In our reconstitution, five components, RyR1, Cav1.1, β1a, JP2 and Stac3, are essential for
229 DICR; removal of each component abolished or reduced the DICR activity (**Fig. 2a, b**). This is
230 consistent with previous findings from mice lacking each component[9,14–16,34]. In addition, the
231 effects of α_2-δ and γ_1 auxiliary subunits on DICR activity corresponded with findings of
232 previous reports [37,38] (**Fig. 2c, d**). Therefore, our reconstituted platform successfully reproduces
233 DICR in skeletal muscle. We found that a substantial DICR still occurred without JP2 (**Fig. 2a,**
234 **b**). This is in contrast to reports by Perni et al.[25,53], in which no voltage-gated Ca^{2+} release was
235 observed in reconstituted cells without junctophilins. A possible reason for this is differences
236 in expression methods. Our VSV-G baculovirus is more effective at transduction than standard
237 lipofection; therefore, sufficient proteins were expressed that might spontaneously interact with
238 each other without junctophilins.

239 We quantitatively evaluated the effect of disease-casing mutations or drugs using the EC_{50}
240 value for [K^+]. In our experimental conditions, the EC_{50} value for K^+ was about 10 mM (**Fig.**
241 **1d**). The value is lower than that for skeletal muscle[54] or myotubes[55] in high [K^+]-induced Ca^{2+}
242 transients. This may be partly explained by measurement differences. We calculated the EC_{50}
243 from the fluorescence intensity for 125–150 seconds after stimulation (**Fig. 1c**). This reduced
244 the EC_{50} by ~7 mM compared with the value obtained just after stimulation (**Supplementary**
245 **Fig. 3**). Nevertheless, our results reproduced the effects of disease-causing mutations (**Fig. 3–**
246 **5**) or drugs (**Fig. 6, 7**), strongly indicating that the EC_{50} value for K^+ is a valid parameter for
247 quantitative evaluation.

248 Formation of DICR machinery can cause peripheral localization of the components, e.g.,
249 RyR1 and Cav1.1, in the reconstituted cells[25,53]. In our reconstituted cells, however, no such
250 peripheral-specific localization was observed; the components were localized throughout cells
251 except for in nuclei (**Supplementary Fig. 1**). This may be because of high levels of the
252 components expressed by baculovirus, which not only accelerates formation of the DICR
253 machinery (as discussed above), but also increases the number of uncoupled components.

254 Mutations in Cav1.1 are implicated in various muscle diseases, including MH and

255 myopathy[12,39]. Among three MH mutations (R174W, R1086H and T1354S), we demonstrated
256 that R1086H, but not R174W orT1354S, significantly accelerated DICR (**Fig. 4c–e**). This is
257 consistent with previous findings using Cav1.1-deficient (dysgenic) myotubes [17–19]. All three
258 mutations show increased sensitivity to caffeine-induced Ca^{2+} release compared with WT,
259 indicating enhanced CICR activity [17–19]. However, we showed that caffeine sensitivity was
260 increased only for R1086H (**Fig. 4f–h**). A possible reason for this difference is the cells used.
261 We used stable RyR1-overexpressing cells. This may cause an excess amount of 'uncoupled'
262 RyR1, which might mask the enhanced sensitivity of caffeine dependence of the 'coupled' RyR1
263 by Cav1.1 mutations.

264 Most myopathy-related mutations identified in Cav1.1 have not been functionally
265 characterized. We evaluated four mutations (E100K, F275L, P742Q and L1367V) found in
266 patients with congenital myopathy[42] (**Fig. 5**). We demonstrated that P742Q substantially
267 inhibited DICR with a large rightward shifted K^+ dependence. This proline resides in the II-III
268 loop which interacts with RyR1 or Stac3[56]. Substitution of the proline to threonine, the residue
269 found in the corresponding position of CaV1.2, diminished DICR in dysgenic myotubes[57].
270 Therefore, P742Q may cause myopathy by reducing DICR activity. E100K and L1367V had
271 no or only minor impacts on DICR activity. These mutations might cause muscle weakness by
272 reasons other than reduced DICR. F275L is recessive because it was found in two compound
273 heterozygous sisters carrying F275L and the nonsense mutation, p.L791Cfs*37[42]. F275L
274 completely abolished DICR without any changes in ER [Ca^{2+}] or caffeine sensitivity. This does
275 not fit with a recessive mutation; if this is the case, patients will have no DICR activity. Further
276 investigations are required for this mutation.

277 There are no specific treatments for most DICR-related diseases; therefore, there is an
278 urgent need to develop novel drugs for these diseases[11–13]. We here evaluated DICR modulators.
279 Among three known RyR1 inhibitors, dantrolene and Cpd1 suppressed DICR (**Fig. 6**). This is
280 consistent with the suppression of twitch and tetanic tensions of isolated muscles and of reduced
281 *in vivo* muscle weakness by dantrolene[46,47] and Cpd1[24]. Interestingly, procaine did not suppress
282 DICR (**Fig. 6**). Procaine inhibits CICR but not DICR in frog skeletal muscle[44] and reconstituted
283 frog α-RyR and β-RyR in RyR1-deficient myotubes[45]. Our data show similar procaine action in
284 a mammalian system. We also demonstrated that lyotropic anions (perchlorate and thiocyanate)
285 accelerate DICR (**Fig. 7**). This reproduces previous findings using skeletal muscle fibers[48–52].
286 Interestingly, lyotropic anions did not affect caffeine dependence, suggesting no effect on CICR
287 (**Fig. 7**). Therefore, our high-throughput platform will also be useful for drug testing and

288 screening for novel drugs that affect DICR.

289 In summary, we established a high-throughput platform for skeletal muscle DICR. This
290 platform will be useful for both evaluation of disease-causing mutations and the development
291 of novel drugs for DICR-related diseases.

292

293 **Methods**

294 **Generation of stable inducible HEK293 cell lines**

295 HEK293 cells stably expressing R-CEPIA1er and RyR1 were generated as described
296 previously[21,22]. Briefly, a full-length rabbit RyR1 cDNA was cloned in a tetracycline-induced
297 expression vector (pcDNA5/FRT/TO; Life Technologies, CA, USA)[58]. Flp-In T-REx HEK293
298 cells were co-transfected with this expression vector and pOG44 in accordance with the
299 manufacturer's instructions. Clones with suitable doxycycline-induced expression of RyR1
300 were selected and used for experiments. The cells were then transfected with an R-CEPIA1er
301 cDNA (a generous gift from Masamitsu Iino, The University of Tokyo) for stable expression of
302 R-CEPIA1er. Cells were cultured in Dulbecco's modified Eagle's medium supplemented with
303 10% fetal calf serum, 2 mM L-glutamine, 15 μg/ml blasticidin, and 100 μg/ml hygromycin.

304 **Production of baculovirus**

305 Baculovirus that expresses vesicular stomatitis virus G-protein (VSVG) on the virus envelope[28]
306 was produced using the Bac-to-Bac system (LifeTechnologies) as described previously[29].
307 cDNAs for Cav1.1, β1a, JP2, Stac3, and Kir2.1 were cloned from mouse skeletal muscle using
308 reverse transcription-PCR (primers pair are listed in **Supplementary Table 1**) and cloned into
309 the modified donor vector (pFastBac1-VSVG-CMV-WPRE). Baculovirus was produced in Sf9
310 cells according to the manufacturer's instructions (LifeTechnologies). Baculovirus titers were
311 immunologically determined using an anti-gp64 antibody (AcV5, Santa Cruz Biotechnology)[59].
312 Titers were $1–2\times10^8$ pfu/mL for all viruses. The baculovirus solutions were stored in the dark
313 at 4°C and used within one month after production.

314 **Immunocytochemistry**

315 RyR1-HEK293 cells infected with baculovirus for the essential components (5 BV cells) were
316 fixed with ice-cold methanol and rinsed with phosphate-buffered saline (PBS). The cells were

317 blocked with 5% BSA/PBS for 30 min and incubated overnight with primary antibodies against
318 Cav1.1 (sc-514685, Santa Cruz Biotechnology), β1a (MA5-27714, Invitrogen), JP2 (sc-377086,
319 Santa Cruz Biotechnology), Stac3 (1G8, Abnova), or Kir2.1 (S112B-14, Invitrogen) in 1%
320 BSA/PBS. After washing three times with PBS, the cells were incubated for 2 h with Alexa594-
321 labeled goat anti-mouse IgG (Invitrogen) in 1% BSA/PBS. After washing with PBS, the cells
322 were observed using an all-in-one fluorescence microscope (BZ-X710, Keyence, Osaka, Japan).

323 **Western blotting**

324 RyR1-HEK293 cells with or without baculovirus infection for the essential components were
325 lysed with Pro-Prep protein extraction solution (iNtRON Biotechnology). The extracted
326 proteins were separated on 3–15% polyacrylamide gels and transferred to PVDF membranes.
327 Membranes were probed with the primary antibodies described above, followed by HRP-
328 labeled anti-mouse IgG (04-18-18, KPL). Positive bands were detected by chemiluminescence
329 using ImmunoStar LD (Fujifilm Wako Chemicals) as a substrate.

330 **Single-cell Ca^{2+} imaging**

331 RyR1/R-CEPPIA1er HEK293 cells grown on a glass-bottomed dish were treated with
332 doxycycline to induce the expression of RyR1 and infected with 5 BV 24 h prior to
333 measurement. Single-cell Ca^{2+} imaging was performed as described previously[29,60].
334 Measurements were performed at 26°C by perfusing solutions using an in-line solution
335 heater/cooler (Warner Instruments, Holliston, MA, USA). ER Ca^{2+} signals were determined by
336 R-CEPIA1er fluorescence excited at 561 nm using a 40× objective lens. Cells were perfused
337 with normal Krebs solution (140 mM NaCl, 5 mM KCl, 2 mM $CaCl_2$, 1 mM $MgCl_2$, 11 mM
338 glucose, 5 mM HEPES, pH 7.4) for 30 s, high [K^+] Krebs solution containing 50 mM K^+ for 50
339 s, and normal Krebs solution for 1.5 min. Fluorescence intensities in individual cells were
340 determined by region of interest (ROI) analysis using AquaCosmos software (Hamamatsu
341 Photonics, Hamamatsu, Japan).
342

343 **Time lapse $[Ca^{2+}]_{ER}$ Measurements using a fluorometer**

344 Time lapse $[Ca^{2+}]_{ER}$ measurements were performed using the FlexStation3 fluorometer
345 (Molecular Devices, San Jose, CA)[21,22]. Stable RyR1/R-CEPIA1er HEK293 cells were seeded
346 on 96-well flat-, clear-bottom black microplates (#3603, Corning, New York, NY) at a density
347 of 3×10^4 cells/well in 100 μL culture medium. One day after seeding, 100 μL culture medium

348 containing 2 μg/mL doxycycline (for induction of RyR1) and baculovirus solutions for Cav1.1,
349 β1a, JP2, Stac3, and Kir2.1 (2 μL each) were added to each well. After 24 h, the culture medium
350 were replaced with 81 μL normal Krebs solution, and the microplate was placed in a
351 FlexStation3 fluorometer preincubated at 37°C. Signals from R-CEPIA1er, which was excited
352 at 560 nm and emitted at 610 nm, were captured every 5 seconds for 150 seconds. Thirty
353 seconds after starting, 54 μL of the high $[K^+]$ or caffeine solution was applied to the cells. The
354 fluorescence change was expressed as F/F_0 in which averaged fluorescence intensity of the last
355 25 seconds (F) was normalized to that of the initial 25 seconds (F_0).

356 For drug testing, compounds were added to normal Krebs solution at the indicated
357 concentrations. For determination of $[Ca^{2+}]_{ER}$, cells were incubated with 81 μL normal Krebs
358 solution, and 54 μL Krebs solution containing 50 mM Ca^{2+} and 50 μM ionomycin was added
359 30 sec after starting (final concentrations of Ca^{2+} and ionomycin were 20 mM and 20 μM,
360 respectively). R-CEPIA1er fluorescence was captured every 10 seconds for 6 min.

361 **Measurement of resting membrane potential**

362 The resting membrane potential of baculovirus-infected RyR1-HEK293 cells with or without
363 Kir2.1 expression was measured under current-clamp conditions in the whole cell configuration
364 of the patch-clamp method with an Axopatch 200B amplifier (Molecular Devices, San Jose,
365 CA). Pipettes were fabricated from borosilicate glass capillaries (Kimble) with a vertical pipette
366 puller (PP-83, Narishige, Tokyo, Japan). Pipettes had series resistance of 3–4 MΩ when filled
367 with the pipette solution containing (in mM) 120 D-glutamate, 20 KCl, 10 NaCl, 0.1 EGTA, 2
368 $MgCl_2$, 3 MgATP, and 5 Hepes (pH 7.4 adjusted with KOH). The series resistance was routinely
369 compensated by ~75% with the amplifier. Bath solution contained (in mM): 140 NaCl, 5 KCl,
370 11 glucose, 2 $CaCl_2$, 1 $MgCl_2$, and 10 Hepes (pH 7.4 adjusted with NaOH). High $[K^+]$ bath
371 solution contained (in mM): 95 NaCl, 50 KCl, 11 glucose, 2 $CaCl_2$, 1 $MgCl_2$, and 10 Hepes (pH
372 7.4 adjusted with NaOH). The resting membrane potential was measured immediately after
373 breaking into cells.

374 **Statistics**

375 Data are presented as means ± SD. Unpaired Student's t test was used for comparisons between
376 two groups. One-way analysis of variance (ANOVA), followed by Dunnett's test, was
377 performed to compare three or more groups. Two-tailed tests were used for all analyses.
378 Statistical analysis was performed using Prism v9 (GraphPad Software, Inc., La Jolla, USA).

Data availability

All data generated or analyzed in this study are available within the article and its Supplementary Information. All raw data supporting the findings from this study are available from the corresponding author upon request. Source data are provided with this paper.

References

1. Franzini-Armstrong C. The relationship between form and function throughout the history of excitation-contraction coupling. J Gen Physiol 150, 189-210 (2018).
2. Rios E, Pizarro G. Voltage sensor of excitation-contraction coupling in skeletal muscle. Physiol Rev 71, 849-908 (1991).
3. Schneider MF. Control of calcium release in functioning skeletal muscle fibers. Annu Rev Physiol 56, 463-484 (1994).
4. Shishmarev D. Excitation-contraction coupling in skeletal muscle: recent progress and unanswered questions. Biophys Rev 12, 143-153 (2020).
5. Flucher BE, Campiglio M. STAC proteins: The missing link in skeletal muscle EC coupling and new regulators of calcium channel function. Biochim Biophys Acta Mol Cell Res 1866, 1101-1110 (2019).
6. Horstick EJ*, et al.* Stac3 is a component of the excitation-contraction coupling machinery and mutated in Native American myopathy. Nat Commun 4, 1952 (2013).
7. Nelson BR*, et al.* Skeletal muscle-specific T-tubule protein STAC3 mediates voltage-induced Ca2+ release and contractility. Proc Natl Acad Sci U S A 110, 11881-11886 (2013).
8. Reinholt BM, Ge X, Cong X, Gerrard DE, Jiang H. Stac3 is a novel regulator of skeletal muscle development in mice. PLoS One 8, e62760 (2013).
9. Takeshima H, Komazaki S, Nishi M, Iino M, Kangawa K. Junctophilins: a novel family of junctional membrane complex proteins. Mol Cell 6, 11-22 (2000).
10. Rufenach B, Van Petegem F. Structure and function of STAC proteins: Calcium channel modulators and critical components of muscle excitation-contraction coupling. J Biol Chem 297, 100874 (2021).
11. Agrawal A, Suryakumar G, Rathor R. Role of defective Ca(2+) signaling in skeletal muscle weakness: Pharmacological implications. J Cell Commun Signal 12, 645-659

411 (2018).
412 12. Flucher BE. Skeletal muscle CaV1.1 channelopathies. Pflugers Arch 472, 739-754
413 (2020).
414 13. Lawal TA, *et al.* Ryanodine receptor 1-related disorders: an historical perspective and
415 proposal for a unified nomenclature. Skelet Muscle 10, 32 (2020).
416 14. Tanabe T, Beam KG, Powell JA, Numa S. Restoration of excitation-contraction
417 coupling and slow calcium current in dysgenic muscle by dihydropyridine receptor
418 complementary DNA. Nature 336, 134-139 (1988).
419 15. Gregg RG, *et al.* Absence of the beta subunit (cchb1) of the skeletal muscle
420 dihydropyridine receptor alters expression of the alpha 1 subunit and eliminates
421 excitation-contraction coupling. Proc Natl Acad Sci U S A 93, 13961-13966 (1996).
422 16. Polster A, Nelson BR, Olson EN, Beam KG. Stac3 has a direct role in skeletal muscle-
423 type excitation-contraction coupling that is disrupted by a myopathy-causing mutation.
424 Proc Natl Acad Sci U S A 113, 10986-10991 (2016).
425 17. Weiss RG, O'Connell KM, Flucher BE, Allen PD, Grabner M, Dirksen RT. Functional
426 analysis of the R1086H malignant hyperthermia mutation in the DHPR reveals an
427 unexpected influence of the III-IV loop on skeletal muscle EC coupling. Am J Physiol
428 Cell Physiol 287, C1094-1102 (2004).
429 18. Eltit JM, *et al.* Malignant hyperthermia susceptibility arising from altered resting
430 coupling between the skeletal muscle L-type Ca2+ channel and the type 1 ryanodine
431 receptor. Proc Natl Acad Sci U S A 109, 7923-7928 (2012).
432 19. Pirone A, *et al.* Identification and functional characterization of malignant hyperthermia
433 mutation T1354S in the outer pore of the Cavalpha1S-subunit. Am J Physiol Cell
434 Physiol 299, C1345-1354 (2010).
435 20. Perez CF, *et al.* Functional and structural characterization of a novel malignant
436 hyperthermia-susceptible variant of DHPR-beta1a subunit (CACNB1). Am J Physiol
437 Cell Physiol 314, C323-C333 (2018).
438 21. Murayama T, *et al.* Efficient High-Throughput Screening by Endoplasmic Reticulum
439 Ca^{2+} Measurement to Identify Inhibitors of Ryanodine Receptor Ca^{2+}-Release Channels.
440 Mol Pharmacol 94, 722-730 (2018).
441 22. Murayama T, Kurebayashi N. Assays for Modulators of Ryanodine Receptor
442 (RyR)/Ca(2+) Release Channel Activity for Drug Discovery for Skeletal Muscle and
443 Heart Diseases. Curr Protoc Pharmacol 87, e71 (2019).
444 23. Mori S, *et al.* Structural development of a type-1 ryanodine receptor (RyR1) Ca(2+)-
445 release channel inhibitor guided by endoplasmic reticulum Ca(2+) assay. Eur J Med

Chem 179, 837-848 (2019).

24. Yamazawa T, *et al.* A novel RyR1-selective inhibitor prevents and rescues sudden death in mouse models of malignant hyperthermia and heat stroke. Nat Commun 12, 4293 (2021).

25. Perni S, Lavorato M, Beam KG. De novo reconstitution reveals the proteins required for skeletal muscle voltage-induced Ca(2+) release. Proc Natl Acad Sci U S A 114, 13822-13827 (2017).

26. Block BA, Imagawa T, Campbell KP, Franzini-Armstrong C. Structural evidence for direct interaction between the molecular components of the transverse tubule/sarcoplasmic reticulum junction in skeletal muscle. J Cell Biol 107, 2587-2600 (1988).

27. Suzuki J, Kanemaru K, Ishii K, Ohkura M, Okubo Y, Iino M. Imaging intraorganellar Ca2+ at subcellular resolution using CEPIA. Nat Commun 5, 4153 (2014).

28. Tani H, Nishijima M, Ushijima H, Miyamura T, Matsuura Y. Characterization of cell-surface determinants important for baculovirus infection. Virology 279, 343-353 (2001).

29. Uehara A, *et al.* Extensive Ca2+ leak through K4750Q cardiac ryanodine receptors caused by cytosolic and luminal Ca2+ hypersensitivity. J Gen Physiol 149, 199-218 (2017).

30. Schredelseker J, Shrivastav M, Dayal A, Grabner M. Non-Ca2+-conducting Ca2+ channels in fish skeletal muscle excitation-contraction coupling. Proc Natl Acad Sci U S A 107, 5658-5663 (2010).

31. DiFranco M, Yu C, Quinonez M, Vergara JL. Inward rectifier potassium currents in mammalian skeletal muscle fibres. J Physiol 593, 1213-1238 (2015).

32. Kirkton RD, Bursac N. Engineering biosynthetic excitable tissues from unexcitable cells for electrophysiological and cell therapy studies. Nat Commun 2, 300 (2011).

33. Zhao Y, *et al.* An expanded palette of genetically encoded Ca(2)(+) indicators. Science 333, 1888-1891 (2011).

34. Takeshima H, *et al.* Excitation-contraction uncoupling and muscular degeneration in mice lacking functional skeletal muscle ryanodine-receptor gene. Nature 369, 556-559 (1994).

35. Catterall WA. Structure and regulation of voltage-gated Ca2+ channels. Annu Rev Cell Dev Biol 16, 521-555 (2000).

36. Flucher BE, Obermair GJ, Tuluc P, Schredelseker J, Kern G, Grabner M. The role of auxiliary dihydropyridine receptor subunits in muscle. J Muscle Res Cell Motil 26, 1-6 (2005).

481 37. Obermair GJ, Kugler G, Baumgartner S, Tuluc P, Grabner M, Flucher BE. The Ca2+
482 channel alpha2delta-1 subunit determines Ca2+ current kinetics in skeletal muscle but
483 not targeting of alpha1S or excitation-contraction coupling. J Biol Chem 280, 2229-
484 2237 (2005).
485 38. Ursu D, Schuhmeier RP, Freichel M, Flockerzi V, Melzer W. Altered inactivation of
486 Ca2+ current and Ca2+ release in mouse muscle fibers deficient in the DHP receptor
487 gamma1 subunit. J Gen Physiol 124, 605-618 (2004).
488 39. Beam TA, Loudermilk EF, Kisor DF. Pharmacogenetics and pathophysiology of
489 CACNA1S mutations in malignant hyperthermia. Physiol Genomics 49, 81-87 (2017).
490 40. Carpenter D*, et al.* The role of CACNA1S in predisposition to malignant hyperthermia.
491 BMC Med Genet 10, 104 (2009).
492 41. Stewart SL, Hogan K, Rosenberg H, Fletcher JE. Identification of the Arg1086His
493 mutation in the alpha subunit of the voltage-dependent calcium channel (CACNA1S) in
494 a North American family with malignant hyperthermia. Clin Genet 59, 178-184 (2001).
495 42. Schartner V*, et al.* Dihydropyridine receptor (DHPR, CACNA1S) congenital myopathy.
496 Acta Neuropathol 133, 517-533 (2017).
497 43. Riazi S, Kraeva N, Hopkins PM. Updated guide for the management of malignant
498 hyperthermia. Can J Anaesth 65, 709-721 (2018).
499 44. Thorens S, Endo M. Calcium-induced calcium release and “depolarization”-induced
500 calcium release: their physiological significance. Proc Jpn Acad 51, 473-478 (1975).
501 45. Kashiyama T, Murayama T, Suzuki E, Allen PD, Ogawa Y. Frog alpha- and beta-
502 ryanodine receptors provide distinct intracellular Ca2+ signals in a myogenic cell line.
503 PLoS One 5, e11526 (2010).
504 46. Leslie GC, Part NJ. The action of dantrolene sodium on rat fast and slow muscle in vivo.
505 Br J Pharmacol 72, 665-672 (1981).
506 47. Meyler WJ, Mols-Thurkow I, Scaf AH, Sargo S, Wesseling H. The effect of dantrolene
507 sodium on rat skeletal muscle in relation to the plasma concentration. Eur J Pharmacol
508 53, 335-342 (1979).
509 48. Luttgau HC, Gottschalk G, Kovacs L, Fuxreiter M. How perchlorate improves
510 excitation-contraction coupling in skeletal muscle fibers. Biophys J 43, 247-249 (1983).
511 49. Delay M, Garcia DE, Sanchez JA. The effects of lyotropic anions on charge movement,
512 calcium currents and calcium signals in frog skeletal muscle fibres. J Physiol 425, 449-
513 469 (1990).
514 50. Huang CL. The differential effects of twitch potentiators on charge movements in frog
515 skeletal muscle. J Physiol 380, 17-33 (1986).

516 51. Csernoch L, Kovacs L, Szucs G. Perchlorate and the relationship between charge
517 movement and contractile activation in frog skeletal muscle fibres. J Physiol 390, 213-
518 227 (1987).
519 52. Gonzalez A, Rios E. Perchlorate enhances transmission in skeletal muscle excitation-
520 contraction coupling. J Gen Physiol 102, 373-421 (1993).
521 53. Perni S, Beam K. Junctophilins 1, 2, and 3 all support voltage-induced Ca2+ release
522 despite considerable divergence. J Gen Physiol 154, (2022).
523 54. Caputo C, Bolanos P. Fluo-3 signals associated with potassium contractures in single
524 amphibian muscle fibres. J Physiol 481 (Pt 1), 119-128 (1994).
525 55. Yang T, *et al.* Pharmacologic and functional characterization of malignant hyperthermia
526 in the R163C RyR1 knock-in mouse. Anesthesiology 105, 1164-1175 (2006).
527 56. Wong King Yuen SM, Campiglio M, Tung CC, Flucher BE, Van Petegem F. Structural
528 insights into binding of STAC proteins to voltage-gated calcium channels. Proc Natl
529 Acad Sci U S A 114, E9520-E9528 (2017).
530 57. Kugler G, Weiss RG, Flucher BE, Grabner M. Structural requirements of the
531 dihydropyridine receptor alpha1S II-III loop for skeletal-type excitation-contraction
532 coupling. J Biol Chem 279, 4721-4728 (2004).
533 58. Tong J, Oyamada H, Demaurex N, Grinstein S, McCarthy TV, MacLennan DH.
534 Caffeine and halothane sensitivity of intracellular Ca2+ release is altered by 15 calcium
535 release channel (ryanodine receptor) mutations associated with malignant hyperthermia
536 and/or central core disease. J Biol Chem 272, 26332-26339 (1997).
537 59. Kitts PA, Green G. An immunological assay for determination of baculovirus titers in
538 48 hours. Anal Biochem 268, 173-178 (1999).
539 60. Murayama T, *et al.* Divergent Activity Profiles of Type 1 Ryanodine Receptor Channels
540 Carrying Malignant Hyperthermia and Central Core Disease Mutations in the Amino-
541 Terminal Region. PLoS One 10, e0130606 (2015).
542

543 **Acknowledgements**

544 We thank Ikue Hiraga and the Laboratory of Proteomics and Biomolecular Science, Biomedical
545 Research Core Facilities, Juntendo University Graduate School of Medicine, for technical
546 assistance. We thank Jeremy Allen, PhD, from Edanz (https://jp.edanz.com/ac) for editing a
547 draft of this manuscript.

548 **Author information**

Affiliations

Department of Pharmacology, Juntendo University School of Medicine, Tokyo, Japan

Takashi Murayama, Nagomi Kurebayashi, Takuya Kobayashi, Satoru Okazaki, Kyosuke Yamashiro and Takashi Sakurai

Department of Molecular Pharmacology, Shinshu University School of Medicine, Matsumoto, Japan.

Takuro Numaga-Tomita, Tsutomu Nakada, and Mitsuhiko Yamada

Institute of Biomaterials and Bioengineering, Tokyo Medical and Dental University, Tokyo, Japan.

Shuichi Mori, Ryosuke Ishida, and Hiroyuki Kagechika

Contributions

T.M. and N.K. conceived and designed the work. T.M., N.K., T.N.-T., S.O., K.Y., S.M., and R.I. acquired and analyzed data. T.M., N.K., T.N.-T., T.K., S.O., K.Y., T.N., S.M., R.I., K.H., M.Y., T.S. interpreted data. T.M. and N.K. wrote the manuscript. All authors reviewed and approved the manuscript.

Corresponding authors

Correspondence to Takashi Murayama (takashim@juntendo.ac.jp).

Ethics declarations

Competing interests

574 The authors declare no competing interests.

575

576 **Figure legends**

577 **Fig. 1. DICR measurements in 96-well plates using a fluorescence microplate reader. a**
578 Schematic drawing of RyR1/R-CEPIA1er HEK293 cells without (No BV, left) and with (5 BV,
579 right) baculovirus infection of essential components for DICR (Cav1.1, β1a, JP2, Stac3) and
580 Kir2.1. **b**, **c** Typical results of time-lapse R-CEPIA1er fluorescence measurement using a
581 FlexStation3 fluorescence microplate reader for RyR1/R-CEPIA1er HEK293 cells without (**b**,
582 No BV) or with (**c**, 5 BV) BV infection. High [K^+] solution ranging from 5–61 mM (symbols
583 shown in **c**) or 10 mM caffeine (light blue) was applied at 30 seconds after starting (blue
584 arrowheads). **d** [K^+] dependence of R-CEPIA1er fluorescence (F/F_0) in No BV (black) and 5
585 BV cells (red). F/F_0 was obtained by normalizing the averaged fluorescence of the last 25
586 seconds (F) to that of the first 25 seconds (F_0). Data are means ± SD (n = 6). **e** Fluorescence
587 change by 61 mM K^+ or 10 mM caffeine. Fluorescence change is expressed as $1-F/F_0$ (see panel
588 **d**). Data are means ± SD (n = 6) and were analyzed by two-way ANOVA with Bonferroni's
589 multiple comparisons test. Note that 5 BV cells show large fluorescence change with high [K^+]
590 which is nearly 80% of that with caffeine.

591 **Fig. 2. Validation of the reconstituted DICR platform. a** K^+ dependence of R-CEPIA1er
592 fluorescence (F/F_0) in 5 BV (black), -Cav1.1 (red), and -JP2 (dark blue). Data are means ± SD
593 (n = 9 for 5 BV, 6 for -Cav1.1 and -JP2). **b** Fluorescence change by 61 mM K^+ in the BV-
594 infected cells lacking one of essential components (-Cav1.1, -β1a, -Stac3, or -JP2) or with RyR2
595 cells instead of RyR1. Data are means ± SD (n = 6) and were analyzed by one-way ANOVA
596 with Dunnett's multiple comparisons test. **c** [K^+] dependence of R-CEPIA1er fluorescence
597 (F/F_0) in cells infected with 5 BV (black), 5 BV plus α_2-δ (+α_2-δ, purple) and 5 BV plus γ1 (+γ1,
598 orange). Data are means ± SD (n = 6). **d** Fluorescence change by 61 mM K^+ in 5 BV, +α_2-δ,
599 and +γ1 cells. Data are means ± SD (n = 6) and were analyzed by one-way ANOVA with
600 Dunnett's multiple comparisons test.

601 **Fig. 3. Effects of Kir2.1 on DICR activity. a, b** Typical results of R-CEPIA1er fluorescence
602 in cells infected with 5 BV (**a**) and BV without Kir2.1 (-Kir2.1) (**b**). High [K^+] solution ranging
603 from 5–61 mM (symbols shown in **a**) was applied at 30 seconds after starting (blue arrowheads).
604 **c** [K^+] dependence of R-CEPIA1er fluorescence (F/F_0) in cells infected 5 BV (black) and BV

605 without Kir2.1 (-Kir2.1) (pink). Data are means ± SD (n = 6). **d** Resting ER [Ca^{2+}] in cells
606 infected with 5 BV (5 BV), BV without Kir2.1 (-Kir2.1), Kir2.1 and β1a (-Kir2.1, -β1a), or
607 Kir2.1 and Stac3 (-Kir2.1, -Stac3). Data are means ± SD (n = 8) and were analyzed by one-way
608 ANOVA with Dunnett's multiple comparisons test. **e** Resting membrane potential of cells
609 infected with 5 BV (left) or BV without Kir2.1 (-Kir2.1) (right). Data are means ± SD (n = 10
610 and 16 for 5 mM and 50 mM K^+, respectively, for 5 BV and 10 and 14 for 5 mM and 50 mM
611 K^+, respectively, for -Kir2.1) and were analyzed by two-way ANOVA with Bonferroni's
612 multiple comparisons test.

613 **Fig. 4. Effect of MH mutations in Cav1.1 on DICR activity. a** Schematic drawing of the
614 location of MH mutations (R174W, R1086H and T1354S) in Cav1.1. **b** Resting ER [Ca^{2+}] in
615 cells expressing WT and mutant Cav1.1. Data are means ± SD (n = 12) and were analyzed by
616 one-way ANOVA with Dunnett's multiple comparisons test. **c** [K^+] dependence of R-CEPIA1er
617 fluorescence (F/F_0) in WT (black), R174W (red), R1086H (blue) and T1354S (green) Cav1.1
618 cells. Data are means ± SD (n = 9). **d, e** Fluorescence change by 61 mM K^+ (**d**) and EC_{50} values
619 for K^+ (**e**). Data are means ± SD (n = 9) and were analyzed by one-way ANOVA with Dunnett's
620 multiple comparisons test. **f** Caffeine dependence of v(F/F_0) in WT (black), R174W (red),
621 R1086H (blue) and T1354S (green) Cav1.1 cells. Data are means ± SD (n = 9). **g, h**
622 Fluorescence change by 20 mM caffeine (**g**) and EC_{50} values for caffeine (**h**). Data are means
623 ± SD (n = 9) and were analyzed by one-way ANOVA with Dunnett's multiple comparisons test.

624 **Fig. 5. Effect of myopathy mutations in Cav1.1 on DICR activity. a** Schematic drawing of
625 the location of myopathy mutations (E100K, F275L, P742Q and L1367V) in Cav1.1. **b** Resting
626 ER [Ca^{2+}] in cells expressing WT and mutant Cav1.1. Data are means ± SD (n = 12) and were
627 analyzed by one-way ANOVA with Dunnett's multiple comparisons test. **c** [K^+] dependence of
628 R-CEPIA1er fluorescence (F/F_0) in WT (black), E100K (red), F275L (blue), P742Q (green)
629 and L1367V (magenta) Cav1.1 cells. Data are means ± SD (n = 9). **d, e** Fluorescence change
630 by 61 mM K^+ (**d**) and EC_{50} values for K^+ (**e**). Data are means ± SD (n = 9) and were analyzed
631 by one-way ANOVA with Dunnett's multiple comparisons test. **f** Caffeine dependence of R-
632 CEPIA1er fluorescence (F/F_0) in WT (black), E100K (red), F275L (blue), P742Q (green) and
633 L1367V (magenta) Cav1.1 cells. Data are means ± SD (n = 9). **g, h** Fluorescence change by 20
634 mM caffeine (**g**) and EC_{50} values for caffeine (**h**). Data are means ± SD (n = 9) and were
635 analyzed by one-way ANOVA with Dunnett's multiple comparisons test.

636 **Fig. 6. Effect of RyR1 inhibitors on DICR activity. a** Chemical structures of dantrolene, Cpd1

637 and procaine. **b** [K^+] dependence of fluorescence change (F/F_0) in cells without (Control, black)
638 or with dantrolene (10 μM, red), Cpd1 (3 μM, blue) or procaine (5 mM, green). Data are means
639 ± SD (n = 9). **c** EC_{50} values for K^+. Data are means ± SD (n = 9) and were analyzed by one-
640 way ANOVA with Dunnett's multiple comparisons test. **d** Caffeine dependence of R-CEPIA1er
641 fluorescence (F/F_0) in cells without (Control, black) or with dantrolene (10 μM, red), Cpd1 (3
642 μM, blue) or procaine (5 mM, green). Data are means ± SD (n = 9). **e** EC_{50} values for caffeine.
643 Data are means ± SD (n = 9) and were analyzed by one-way ANOVA with Dunnett's multiple
644 comparisons test.

645 **Fig. 7. Effect of lyotropic anions on DICR activity. a** [K^+] dependence of fluorescence change
646 (F/F_0) in cells in the absence (Control, black) or presence of perchlorate (10 mM, red) or
647 thiocyanate (10 mM, blue). Data are means ± SD (n = 9). **b** EC_{50} values for K^+. Data are means
648 ± SD (n = 9) and were analyzed by one-way ANOVA with Dunnett's multiple comparisons test.
649 **c** Caffeine dependence of R-CEPIA1er fluorescence (F/F_0) in cells in the absence (Control,
650 black) or presence of perchlorate (10 mM, red) or thiocyanate (10 mM, blue). Data are means
651 ± SD (n = 9). **d** EC_{50} values for caffeine. Data are means ± SD (n = 9) and were analyzed by
652 one-way ANOVA with Dunnett's multiple comparisons test.

Fig. 1

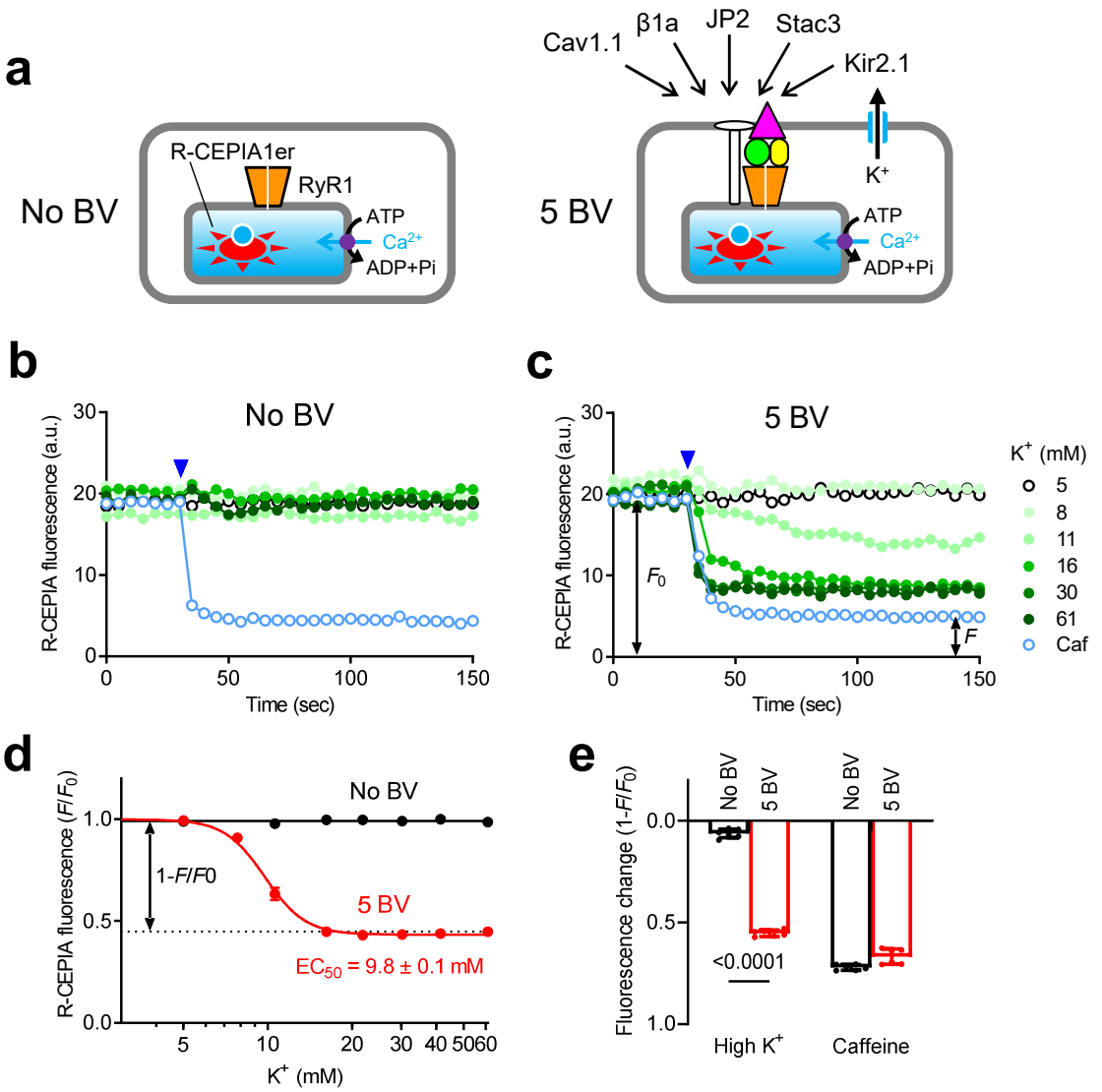

Fig. 1. DICR measurements in 96-well plates using a fluorescence microplate reader. a Schematic drawing of RyR1/R-CEPIA1er HEK293 cells without (No BV, left) and with (5 BV, right) baculovirus infection of essential components for DICR (Cav1.1, β1a, JP2, Stac3) and Kir2.1. **b**, **c** Typical results of time-lapse R-CEPIA1er fluorescence measurement using a FlexStation3 fluorescence microplate reader for RyR1/R-CEPIA1er HEK293 cells without (**b**, No BV) or with (**c**, 5 BV) BV infection. High [K^+] solution ranging from 5–61 mM (symbols shown in **c**) or 10 mM caffeine (light blue) was applied at 30 seconds after starting (blue arrowheads). **d** [K^+] dependence of R-CEPIA1er fluorescence (F/F_0) in No BV (black) and 5 BV cells (red). F/F_0 was obtained by normalizing the averaged fluorescence of the last 25 seconds (F) to that of the first 25 seconds (F_0). Data are means ± SD (n = 6). **e** Fluorescence change by 61 mM K^+ or 10 mM caffeine. Fluorescence change is expressed as $1-F/F_0$ (see panel **d**). Data are means ± SD (n = 6) and were analyzed by two-way ANOVA with Bonferroni's multiple comparisons test. Note that 5 BV cells show large fluorescence change with high [K^+] which is nearly 80% of that with caffeine.

Fig. 2

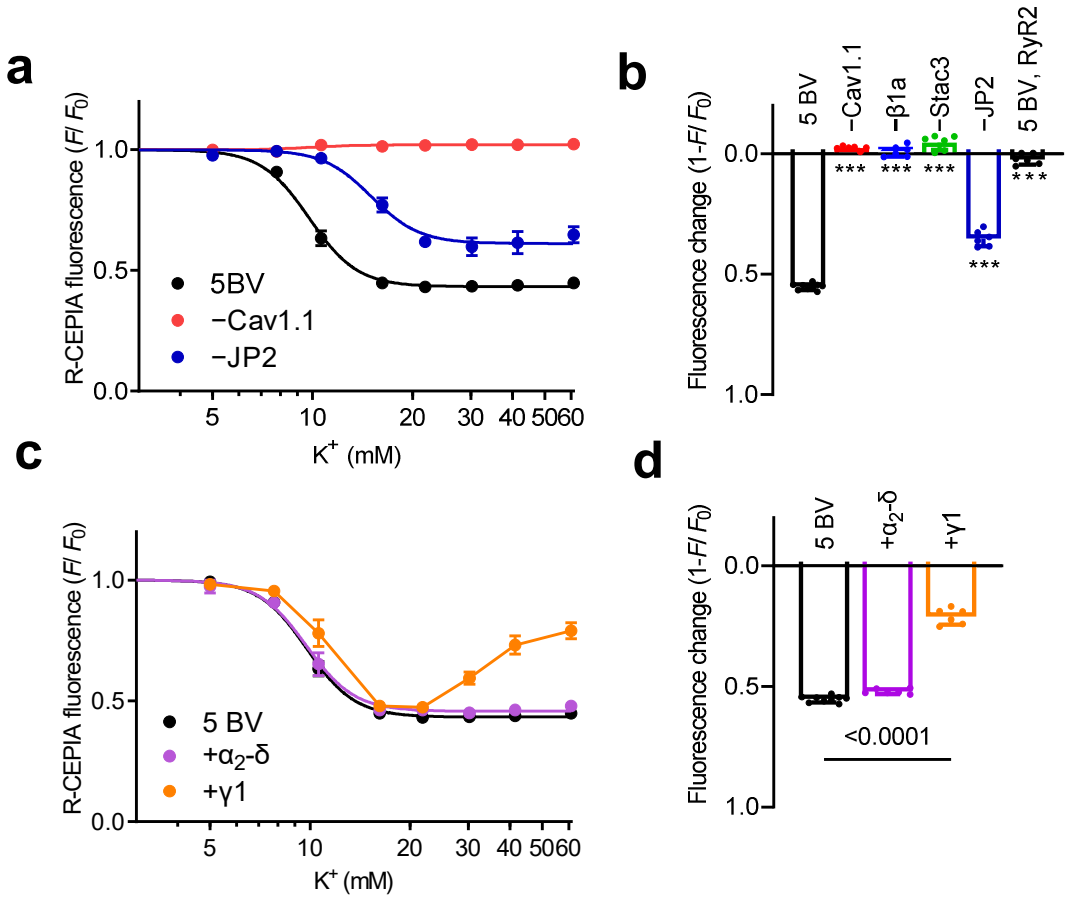

Fig. 2. Validation of the reconstituted DICR platform. a K^+ dependence of R-CEPIA1er fluorescence (F/F_0) in 5 BV (black), -Cav1.1 (red), and -JP2 (dark blue). Data are means ± SD (n = 9 for 5 BV, 6 for -Cav1.1 and -JP2). **b** Fluorescence change by 61 mM K^+ in the BV-infected cells lacking one of essential components (-Cav1.1, -β1a, -Stac3, or -JP2) or with RyR2 cells instead of RyR1. Data are means ± SD (n = 6) and were analyzed by one-way ANOVA with Dunnett's multiple comparisons test. **c** [K^+] dependence of R-CEPIA1er fluorescence (F/F_0) in cells infected with 5 BV (black), 5 BV plus α_2-δ (+α_2-δ, purple) and 5 BV plus γ1 (+γ1, orange). Data are means ± SD (n = 6). **d** Fluorescence change by 61 mM K^+ in 5 BV, +α_2-δ, and +γ1 cells. Data are means ± SD (n = 6) and were analyzed by one-way ANOVA with Dunnett's multiple comparisons test.

Fig. 3

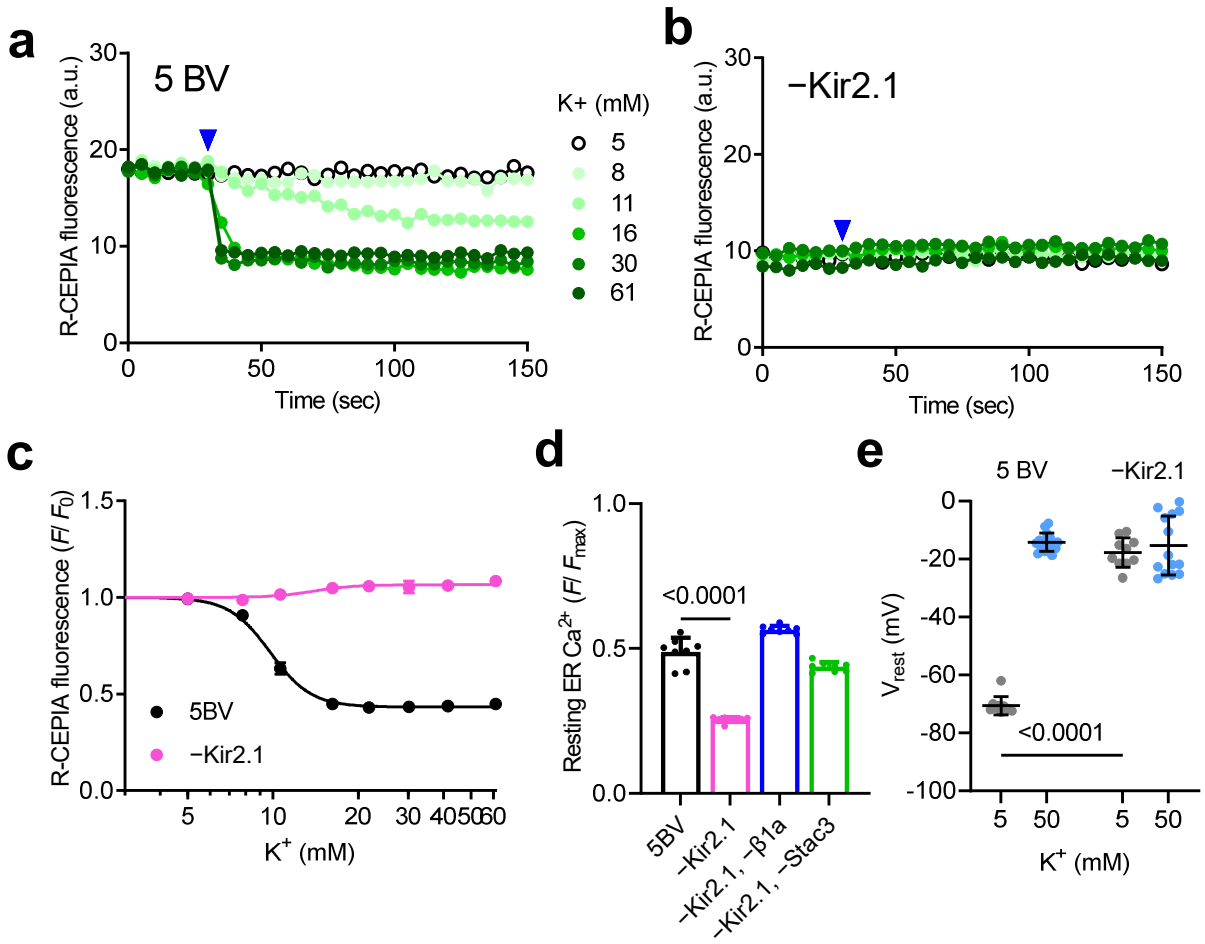

Fig. 3. Effects of Kir2.1 on DICR activity. a, b Typical results of R-CEPIA1er fluorescence in cells infected with 5 BV (**a**) and BV without Kir2.1 (-Kir2.1) (**b**). High [K^+] solution ranging from 5–61 mM (symbols shown in **a**) was applied at 30 seconds after starting (blue arrowheads). **c** [K^+] dependence of R-CEPIA1er fluorescence (F/F_0) in cells infected 5 BV (black) and BV without Kir2.1 (-Kir2.1) (pink). Data are means ± SD (n = 6). **d** Resting ER [Ca^{2+}] in cells infected with 5 BV (5 BV), BV without Kir2.1 (-Kir2.1), Kir2.1 and β1a (-Kir2.1, -β1a), or Kir2.1 and Stac3 (-Kir2.1, -Stac3). Data are means ± SD (n = 8) and were analyzed by one-way ANOVA with Dunnett's multiple comparisons test. **e** Resting membrane potential of cells infected with 5 BV (left) or BV without Kir2.1 (-Kir2.1) (right). Data are means ± SD (n = 10 and 16 for 5 mM and 50 mM K^+, respectively, for 5 BV and 10 and 14 for 5 mM and 50 mM K^+, respectively, for -Kir2.1) and were analyzed by two-way ANOVA with Bonferroni's multiple comparisons test.

Fig. 4

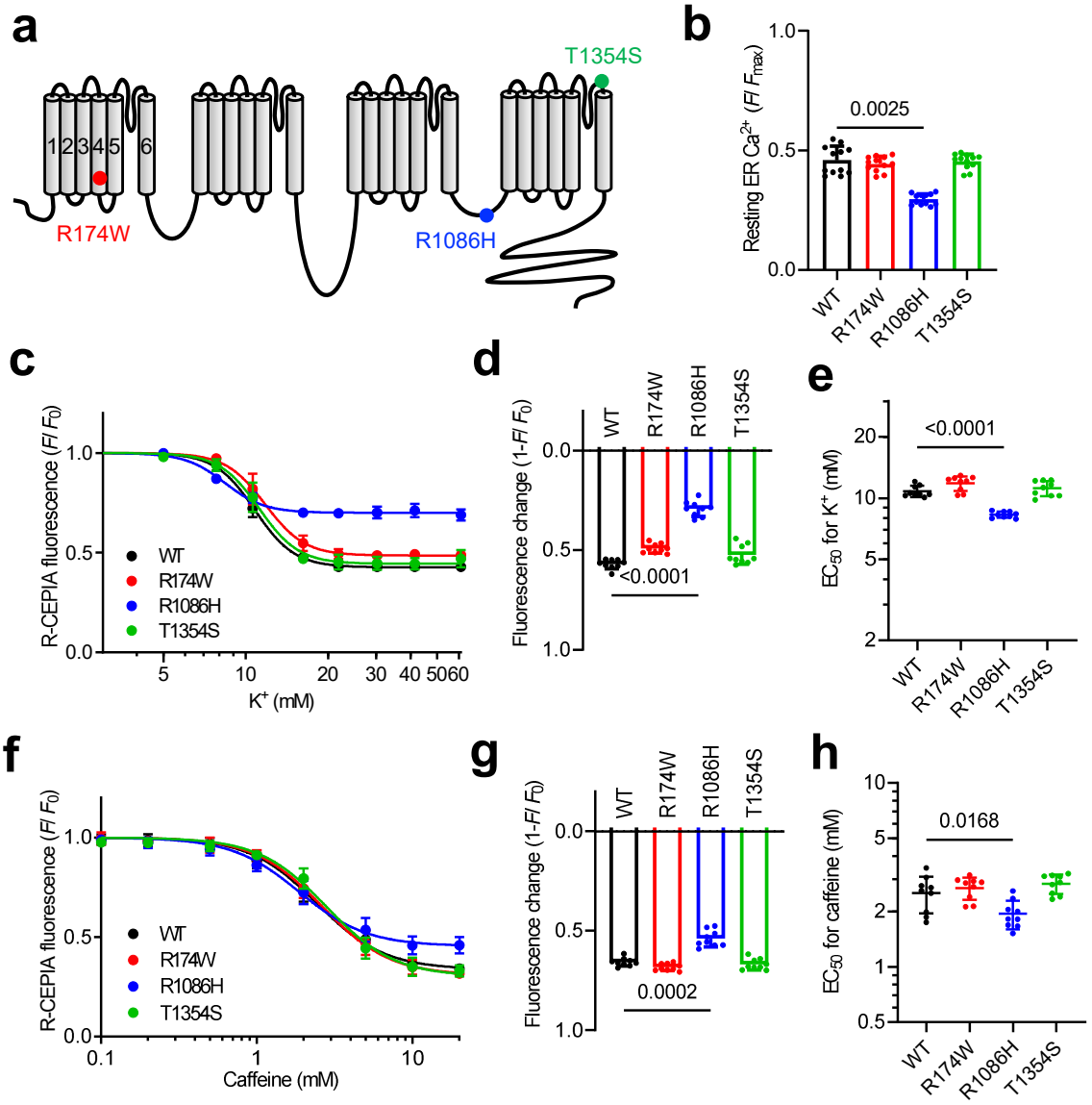

Fig. 4. Effect of MH mutations in Cav1.1 on DICR activity. a Schematic drawing of the location of MH mutations (R174W, R1086H and T1354S) in Cav1.1. **b** Resting ER [Ca^{2+}] in cells expressing WT and mutant Cav1.1. Data are means ± SD (n = 12) and were analyzed by one-way ANOVA with Dunnett's multiple comparisons test. **c** [K^+] dependence of R-CEPIA1er fluorescence (F/F_0) in WT (black), R174W (red), R1086H (blue) and T1354S (green) Cav1.1 cells. Data are means ± SD (n = 9). **d, e** Fluorescence change by 61 mM K^+ (**d**) and EC_{50} values for K^+ (**e**). Data are means ± SD (n = 9) and were analyzed by one-way ANOVA with Dunnett's multiple comparisons test. **f** Caffeine dependence of v(F/F_0) in WT (black), R174W (red), R1086H (blue) and T1354S (green) Cav1.1 cells. Data are means ± SD (n = 9). **g, h** Fluorescence change by 20 mM caffeine (**g**) and EC_{50} values for caffeine (**h**). Data are means ± SD (n = 9) and were analyzed by one-way ANOVA with Dunnett's multiple comparisons test.

Fig. 5

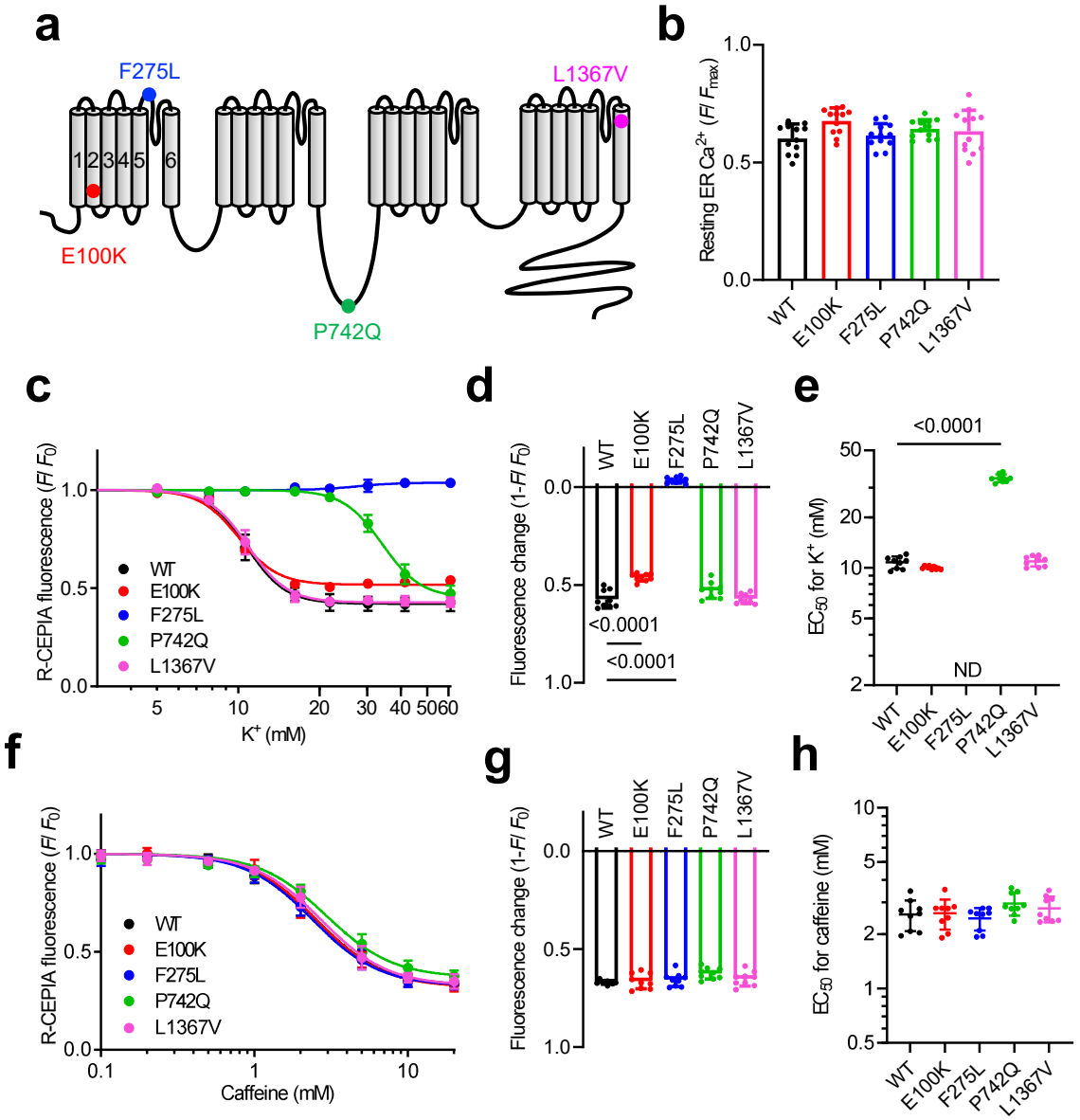

Fig. 5. Effect of myopathy mutations in Cav1.1 on DICR activity. a Schematic drawing of the location of myopathy mutations (E100K, F275L, P742Q and L1367V) in Cav1.1. **b** Resting ER [Ca^{2+}] in cells expressing WT and mutant Cav1.1. Data are means ± SD (n = 12) and were analyzed by one-way ANOVA with Dunnett's multiple comparisons test. **c** [K^+] dependence of R-CEPIA1er fluorescence (F/F_0) in WT (black), E100K (red), F275L (blue), P742Q (green) and L1367V (magenta) Cav1.1 cells. Data are means ± SD (n = 9). **d, e** Fluorescence change by 61 mM K^+ (**d**) and EC_{50} values for K^+ (**e**). Data are means ± SD (n = 9) and were analyzed by one-way ANOVA with Dunnett's multiple comparisons test. **f** Caffeine dependence of R-CEPIA1er fluorescence (F/F_0) in WT (black), E100K (red), F275L (blue), P742Q (green) and L1367V (magenta) Cav1.1 cells. Data are means ± SD (n = 9). **g, h** Fluorescence change by 20 mM caffeine (**g**) and EC_{50} values for caffeine (**h**). Data are means ± SD (n = 9) and were analyzed by one-way ANOVA with Dunnett's multiple comparisons test.

Fig. 6

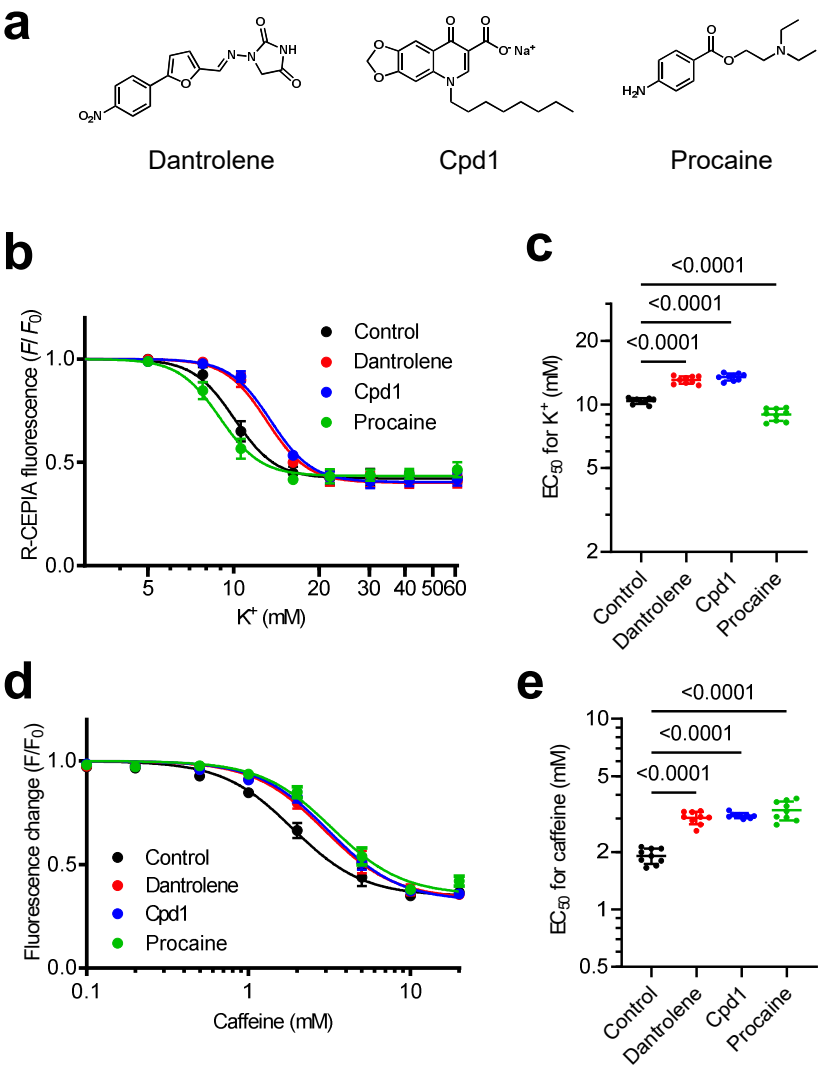

Fig. 6. Effect of RyR1 inhibitors on DICR activity. a Chemical structures of dantrolene, Cpd1 and procaine. **b** [K^+] dependence of fluorescence change (F/F_0) in cells without (Control, black) or with dantrolene (10 μM, red), Cpd1 (3 μM, blue) or procaine (5 mM, green). Data are means ± SD (n = 9). **c** EC_{50} values for K^+. Data are means ± SD (n = 9) and were analyzed by one-way ANOVA with Dunnett's multiple comparisons test. **d** Caffeine dependence of R-CEPIA1er fluorescence (F/F_0) in cells without (Control, black) or with dantrolene (10 μM, red), Cpd1 (3 μM, blue) or procaine (5 mM, green). Data are means ± SD (n = 9). **e** EC_{50} values for caffeine. Data are means ± SD (n = 9) and were analyzed by one-way ANOVA with Dunnett's multiple comparisons test.

Fig. 7

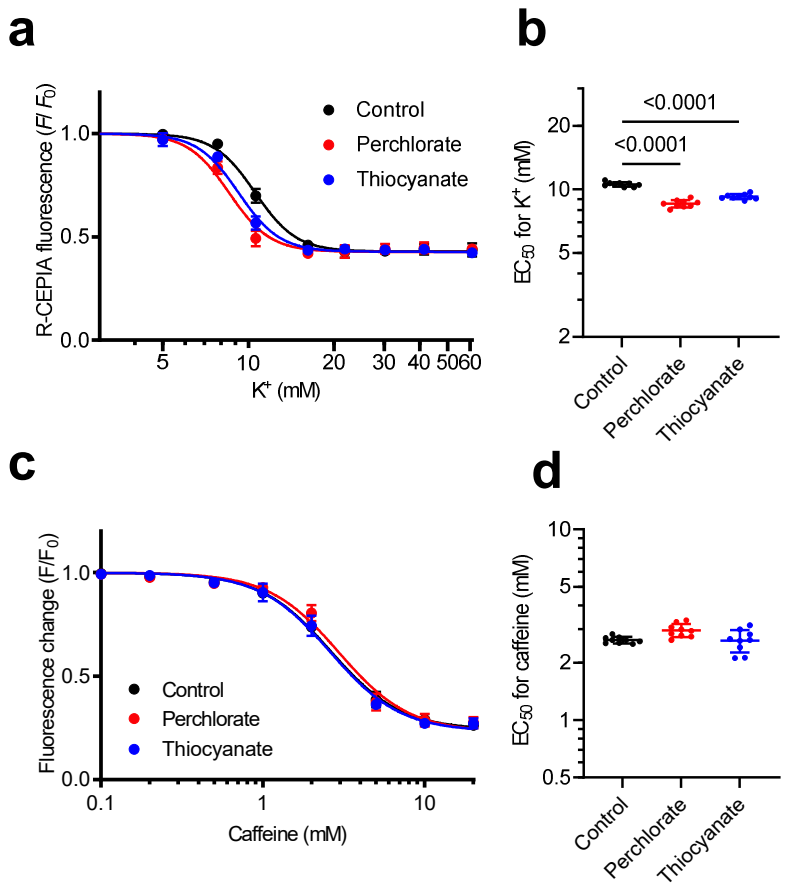

Fig. 7. Effect of lyotropic anions on DICR activity. a [K^+] dependence of fluorescence change (F/F_0) in cells in the absence (Control, black) or presence of perchlorate (10 mM, red) or thiocyanate (10 mM, blue). Data are means ± SD (n = 9). **b** EC_{50} values for K^+. Data are means ± SD (n = 9) and were analyzed by one-way ANOVA with Dunnett's multiple comparisons test. **c** Caffeine dependence of R-CEPIA1er fluorescence (F/F_0) in cells in the absence (Control, black) or presence of perchlorate (10 mM, red) or thiocyanate (10 mM, blue). Data are means ± SD (n = 9). **d** EC_{50} values for caffeine. Data are means ± SD (n = 9) and were analyzed by one-way ANOVA with Dunnett's multiple comparisons test.